ACS OMEGA

http://pubs.acs.org/journal/acsodf

Article

Growth of Single-Walled Carbon Nanotubes from Solid Carbon Nanoparticle Seeds via Cap Formation Engineering with a Two-Step Growth Process and Water Vapor Supply

Mengyue Wang, Keisuke Nakamura, Michiharu Arifuku, Noriko Kiyoyanagi, Taiki Inoue, and Yoshihiro Kobayashi*

Cite This: *ACS Omega* 2022, 7, 3639−3648

Read Online

ACCESS | Metrics & More | Article Recommendations | Supporting Information

ABSTRACT: Solid carbon nanoparticles are promising growth seeds to prepare single-walled carbon nanotubes (SWCNTs) at high temperatures, at which the SWCNT crystallinity should be improved significantly but conventional metal catalyst nanoparticles are unstable and suffer from aggregation. The noncatalytic nature of solid carbon nanoparticles, however, makes SWCNT growth inefficient, resulting in a limited growth yield. In this study, we develop a two-step chemical vapor deposition process to efficiently synthesize high-crystallinity SWCNTs at high temperatures from solid carbon nanoparticles obtained from nanodiamond. Based on thermodynamic considerations, the growth conditions are separately adjusted to supply different growth driving forces which are suitable for the formation of the initial cap structures and for the stationary elongation of SWCNTs. This process, called cap formation engineering, improves the nucleation density of the cap structures. We examined the changes in crystallinity, amorphous carbon deposition, diameter, and yield of SWCNTs with respect to the synthesis conditions. By controlling the initial growth conditions, high-quality SWCNTs are grown with improved yield. With the addition of water vapor as the etchant, deposition of amorphous carbon at high temperatures was further prevented. The results provide a pathway for precise growth control of SWCNTs from unconventional solid growth seeds.

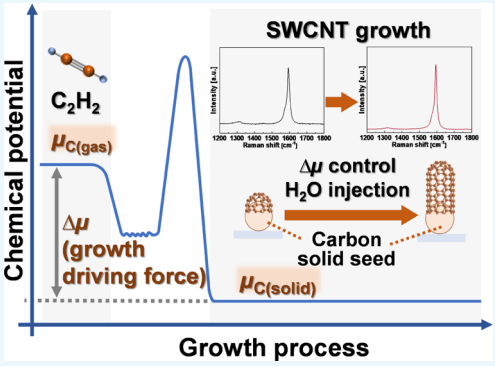

1. INTRODUCTION

Carbon nanotubes (CNTs),[1] which are a quasi-one-dimensional nanomaterials whose structures are formed by seamlessly rolling up single-layer or multilayer graphene sheets, offer diverse excellent properties and are promising for mechanical,[2] electronic,[3] and thermal applications.[4] Especially, single-walled CNTs (SWCNTs)[5] have received increasing attention toward logic circuits,[6] chemical sensors,[7] and quantum light sources[8] due to their superior performances and chirality-dependent optoelectronic properties.[9] Various methods have been developed to obtain SWCNTs. Examples include arc discharge,[10] laser ablation,[11] and chemical vapor deposition (CVD).[12] In such growth processes, carbon atoms decomposed from carbon source molecules are bonded together on a suitable growth seed, which is a nanoparticle acting as a template, to initially form a hemispherical graphitic structure, which is called a cap structure. After the lift-off of the cap structure from the growth seed, a tube structure gradually elongates with the attachment of carbon atoms at the interface of the tube edge and the growth seed.[13] Due to the high degree of freedom of the growth parameters and the excellent compatibility with large-scale production, the CVD process has been extensively studied to realize structure-controlled and high-yield synthesis of SWCNTs.[14−17]

Unfortunately, large discrepancies remain between experimentally synthesized SWCNTs and ideal SWCNTs, which are required for applications in terms of crystallinity, chirality, length, etc. The crystallinity of SWCNTs is one of the most important aspects because structural defects formed on SWCNTs drastically change the electronic structure[18,19] and deteriorate their superior properties, including electrical transport,[18,20,21] thermal transport,[22] and mechanical strength.[23] To achieve highly crystalline SWCNTs, high-temperature CVD processes are effective because the activation barrier for healing defects must be overcome.[24,25] For high growth temperature, growth seeds for SWCNTs require high temperature stability to prevent aggregation phenomena. Catalytic metal nanoparticles, including iron,[26,27] nickel,[28] cobalt,[29] and relevant alloys,[30] are widely used as growth seeds. However, they suffer from deactivation induced

Received: November 7, 2021
Accepted: January 11, 2022
Published: January 20, 2022

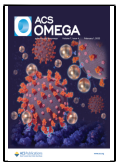

https://doi.org/10.1021/acsomega.1c06268
ACS Omega 2022, 7, 3639−3648

by aggregation due to their moderate melting points, limiting the yield of SWCNTs at high temperature.[31] At the same time, the post-treatment step to exclude metal impurities from as-grown SWCNTs is needed for some applications, but it induces the formation of additional defects.[32]

Recently, nonmetallic nanoparticles with higher melting points have been utilized as growth seeds of SWCNTs.[33−37] Among them, nanodiamond (ND)[38] is a promising growth seed due to its nonfusion characteristic, which prevents aggregation or sintering of nanoparticles even at high growth temperatures. In addition, as-grown SWCNTs from ND nanoparticles are highly pure in terms of elemental composition, mitigating the need for postgrowth purification. One study successfully synthesized highly crystalline SWCNTs at 1000 °C using solid carbon nanoparticles derived from NDs as growth seeds.[39] However, the yield of high-quality SWCNTs is still low at high growth temperatures. It has been reported that increasing the growth temperature makes it more difficult to organize SWCNTs.[39]

The change in the growth efficiency as a function of temperature can be explained by thermodynamic considerations. The growth driving force $\Delta\mu$ is the difference between the chemical potential μ of carbon atoms in carbon feedstock molecules in the gas phase $\mu_{C(gas)}$ and that of carbon atoms in SWCNTs in the solid phase $\mu_{C(solid)}$, which is expressed as $\Delta\mu = \mu_{C(gas)} - \mu_{C(solid)}$ (Figure S3). Both the growth temperature and the carbon source partial pressure affect $\Delta\mu$.[40] Since μ is equal to the partial molar Gibbs energy, when pressure p is kept constant and temperature T is changed, the variation of μ is proportional to the partial molar entropy S_m according to the equation $\left(\frac{\partial \mu}{\partial T}\right)_p = -S_m$. Because S_m in the gas phase is higher than that in the solid phase and $\mu_{C(gas)}$ decreases more drastically than $\mu_{C(solid)}$ as the growth temperature increases, these result in a reduction of $\Delta\mu$ at higher temperatures (Figure S3c). Such a decrease in $\Delta\mu$ at high temperatures makes the formation of SWCNTs difficult, especially for cap structures with a higher strain energy, which exceeds $\mu_{C(solid)}$.[24] As another influential factor, the change in the carbon source partial pressure mainly affects $\mu_{C(gas)}$. A higher carbon source partial pressure increases $\mu_{C(gas)}$, which increases $\Delta\mu$ (Figure S3d).

Since SWCNT growth begins with the cap formation process, optimizing the cap formation condition for a higher nucleation efficiency is necessary to increase the SWCNT growth yield. Thus, an increase in the partial pressure of the carbon feedstock or a decrease in the growth temperature only at the beginning of SWCNT growth should compensate for the high driving force required for cap structure nucleation. After the efficient formation of the cap structures, a moderate driving force should be supplied for subsequent growth of the nanotube sidewalls by controlling the growth condition. The details of driving force required for the different growth stages will be explained in Section 3.2. A two-step growth approach has been employed in SWCNT synthesis using conventional metal nanoparticles at a moderate temperature.[41] However, so far, the effectiveness of two-step growth has scarcely been investigated for a solid seed-supported growth system of SWCNTs, where a unique vapor−solid surface−solid (VSSS) growth mechanism[37,38] takes place rather than vapor−liquid−solid (VLS) model[42,43] employed for metal catalyst-based growth. Although our previous study reported a preliminary result on two-step growth from solid carbon seeds by temporally changing the carbon feeding rate,[44] a more thorough investigation on the cap formation process should realize an efficient synthesis of high-crystallinity SWCNTs and shed light on the unconventional growth mechanism of SWCNTs from solid carbon nanoparticles.

Another factor that prevents the growth of SWCNTs is the deposition of amorphous carbon (a-C), which tends to form under the conditions of high temperature and high carbon feeding rates. In metal catalyst-based CNT growth, with the introduction of water vapor, it has been reported that the activity and lifetime of the metal catalyst were enhanced by selective etching of a-C. The improvement of catalyst property during growth enables a highly efficient synthesis of CNTs and results in massive or superlong CNT growth from metal nanoparticles.[15,45−49] Thus, water-induced etching of a-C has the potential to be utilized in the growth of SWCNTs from solid carbon seeds.

In this work, a two-step approach is developed to efficiently synthesize high-quality SWCNTs using ND-based solid carbon nanoparticles as growth seeds at high temperatures. The effects of growth temperature, carbon feedstock partial pressure, and growth time during the initial growth step on the nucleation of SWCNT caps are investigated to enhance the synthesis from nonmetallic nanoparticles. Following the highly efficient cap formation stage, the carbon supply is reduced to adjust the growth driving force during the secondary growth step at a high temperature. Stationary elongation of tubes in the secondary growth step increases the growth yield of SWCNTs with high crystallinity. Furthermore, highly crystalline impurity-free SWCNTs are obtained with an improved growth yield by introducing water vapor as an etchant just after the formation of the SWCNT cap structures.

2. EXPERIMENTAL SECTION

2.1. Growth Seed Preparation. Figure 1 depicts the whole process, including the pretreatment step of growth seeds and the two-step growth process with and without using water. Purified ND particles (impurity concentrations of 80 ppm for Fe, 2100 ppm for Zr, and 6−20 ppm for Pd) prepared by the detonation method[50,51] were dispersed in ethanol (2.0 wt %) and used as the starting material of the seeds for SWCNT growth. It should be noted that we performed a separate

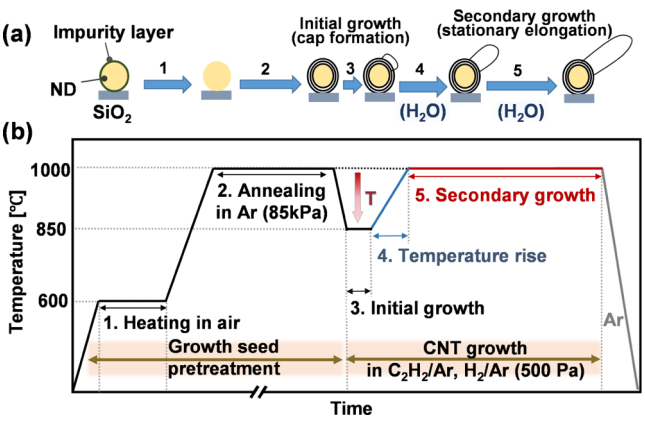

Figure 1. (a) Schematic diagram of the growth seed pretreatment and the two-step growth process of SWCNTs from solid carbon nanoparticles. (b) Temperature profile of the reaction furnace as a function of processing time.

https://doi.org/10.1021/acsomega.1c06268
ACS Omega 2022, 7, 3639−3648

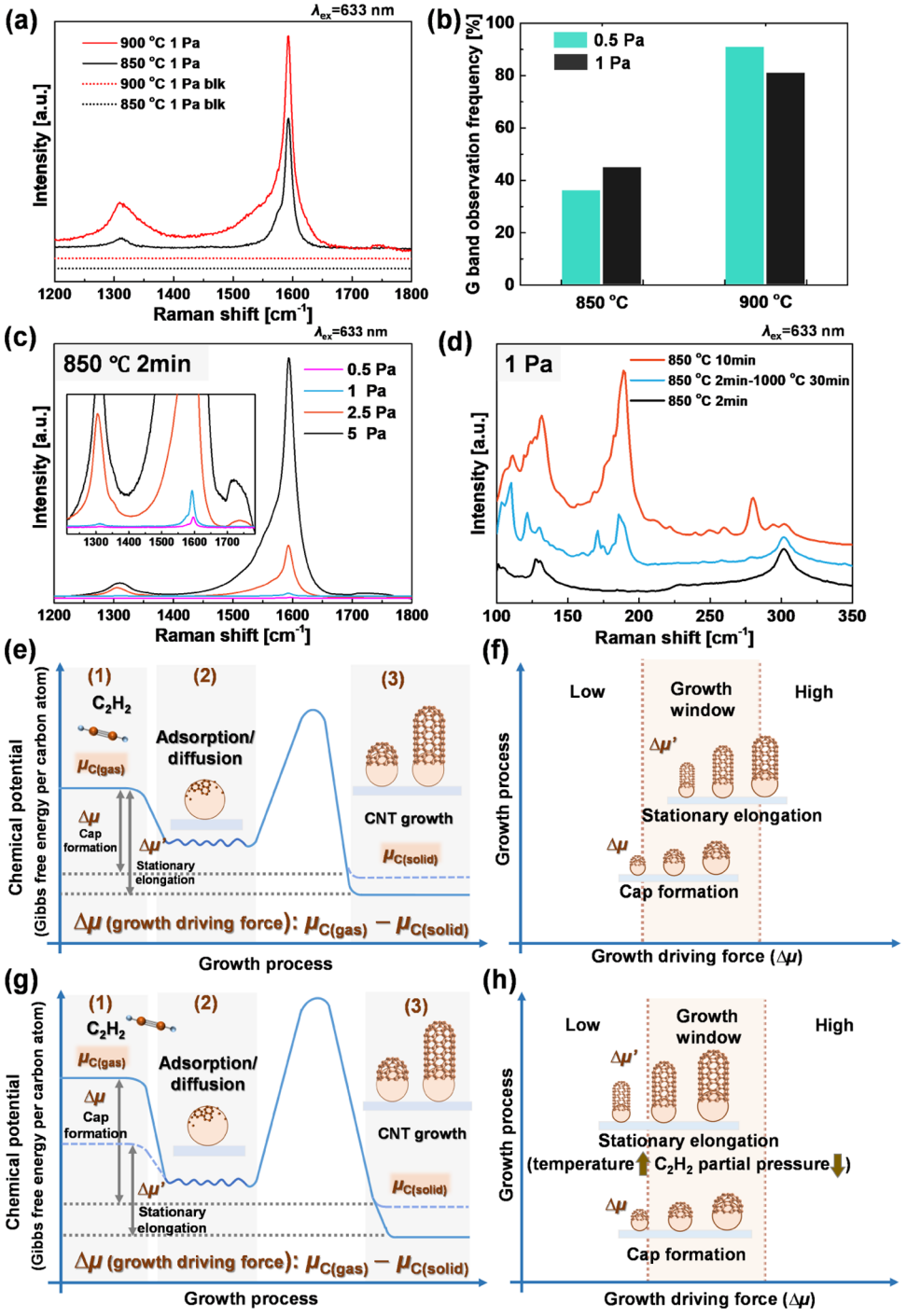

Figure 2. Dependence of the initial growth conditions on the structure and yield of SWCNTs. (a) Raman spectra of SWCNTs grown at 850 and 900 °C with C_2H_2 partial pressure of 1 Pa for 2 min. Dotted lines denote Raman spectra of the blank samples obtained under the same conditions. (b) G band observation frequency of SWCNTs synthesized at 850 and 900 °C with a carbon source partial pressure of 0.5 and 1 Pa for 2 min, which represents the growth yield of SWCNTs. (c) Raman spectra of SWCNTs grown at different carbon source partial pressures: 0.5, 1, 2.5, and 5 Pa. The growth temperature is 850 °C, and the growth time is 2 min. Inset shows magnified spectra. (d) Radial breathing mode (RBM) peaks in Raman spectra of SWCNTs synthesized through only the initial growth step of 850 °C, 1 Pa, and 2 min (denoted as 850 °C 2 min) and 850 °C, 1 Pa, and 10 min (850 °C 10 min) as well as through the initial growth step of 850 °C, 1 Pa, and 2 min followed by the secondary growth step of 1000 °C, 0.5 Pa, and 30 min (850 °C 2 min−1000 °C 30 min). (e) Reaction coordinate and different growth driving force for the cap formation ($\Delta\mu$, solid line) and the stationary elongation ($\Delta\mu'$, dotted line) by only initial growth step (fixed growth condition). (f) Schematic of growth driving force variation for the cap formation and the stationary elongation with different diameters by only initial growth step. (g) Reaction coordinate and different growth driving force by the two-step growth. Growth driving force for the cap formation in the initial growth step ($\Delta\mu$, solid line) and the stationary elongation in the secondary growth step ($\Delta\mu'$, dotted line) is shown. (h) Schematic of growth driving force variation for the cap formation and the stationary elongation with different diameters by the two-step growth.

https://doi.org/10.1021/acsomega.1c06268
ACS Omega 2022, 7, 3639−3648

experiment and confirmed that SWCNTs were grown not from metal impurity contained in purified ND but from solid carbon nanoparticles which were transformed from ND (Figure S1).

Si substrates with a 300 nm thick thermal oxide layer were cut into an ∼10 mm square and cleaned by an ozone treatment process (L-UV253, Japan Electronics Industry) by flowing 6 L/min oxygen for 5 min under ultraviolet light for 60 min followed by exhausting with 6 L/min nitrogen for 5 min. After ultrasonic dispersion, 20 μL of the ND solution was dropped on the surface of the Si substrates. Additionally, the same Si substrates without any growth seeds were used as a reference to examine the amount of a-C deposited directly on substrates (hereafter called blank samples).

2.2. Two-Step Growth Process without Water Vapor Injection. A tubular CVD furnace (GE-1000, GII Techno) was used for pretreatment of the growth seeds and the synthesis of SWCNTs. After the substrate was placed at the center of the quartz tube chamber which had a semicircle cross section with a diameter of 43.6 mm and whose heating zone length is 890 mm, the surface cleaning process was held while heating in air for 10 min at 600 °C to remove various impurities on the substrate and the surface of ND (Figure 1b, process 1). During this process, the diameter of ND was reduced to the appropriate size for SWCNT growth,[38] and the size variation is presented in Figure S2. Further treatment was followed by gradually increasing the furnace temperature to 1000 °C and keeping it at 1000 °C for 1 h as an annealing procedure under the condition of Ar at 85 kPa (Figure 1b, process 2). This step should change the surface of ND (sp^3 carbon) into a more stable graphitic shell (sp^2 carbon), which is called the carbon nano-onion structure.[52,53]

To adjust the growth condition suitable for the initial growth step, where the cap structures are formed, the growth temperature was set to 850 or 900 °C after the aforementioned annealing process at 1000 °C (Figure 1b, process 3). Once the temperature dropped to the set value, which was determined based on the previous high-temperature SWCNT synthesis condition,[39] the pressure was decreased to 500 Pa while continuously injecting Ar at 20 sccm and kept for 3 min for environment stabilization. After that, the gas condition was switched to a 20 sccm mass flow mixture of C_2H_2 (2%)/Ar (1−10 sccm) and H_2 (3%)/Ar (10−19 sccm), while the total pressure was kept at 500 Pa, corresponding to a C_2H_2 partial pressure of 0.5−5 Pa. The typical flow rates of C_2H_2/Ar and H_2/Ar were 2 and 18 sccm, respectively, corresponding to a C_2H_2 partial pressure of 1 Pa. The process lasted for 1 or 2 min as the cap growth stage. Before moving into the secondary growth step, the growth temperature was increased to 1000 °C while controlling the gas mixture to 1 sccm C_2H_2 (2%)/Ar and 19 sccm of H_2 (3%)/Ar, where the partial pressure of C_2H_2 was 0.5 Pa (Figure 1b, process 4). The secondary growth step, where stationary elongation of SWCNTs should occur, began when the growth temperature reached 1000 °C and continued for 30 min while keeping the same gas-phase mixture and pressure conditions (Figure 1b, process 5). Under some experiments, only the initial growth step was conducted, and the temperature was decreased after the 1 or 2 min growth at 850 or 900 °C without the secondary growth step.

2.3. Two-Step Growth Process with Water Vapor Injection. Water vapor was added in some experiments as a growth enhancer because the vapor may prevent the deposition of a-C. Based on the two-step growth process presented above, water vapor typically at 0.15 Pa was injected into the gas phase environment. We started supplying water at two different timings: from the beginning of the temperature rising step and from the beginning of the secondary growth step. The details are explained in Section 3.4.

2.4. Structure Characterization and Yield Evaluation of Synthesized SWCNTs. We analyzed the structure of the synthesized SWCNTs with Raman spectroscopy. A Raman spectrometer (LabRAM HR800, HORIBA Jobin Yvon) was used with an excitation wavelength λ_{ex} of 633 nm. The laser spot size was about 0.9 μm, and the laser power was around 7 mW at the measurement point. The exposure time of each measurement spot was 1 s for five cycles. Raman spectra were collected from 30 randomly selected spots on each sample, and the average spectra were used for further analysis. The quality of formed SWCNTs was discussed by comparing the intensity ratio of the G band (∼1590 cm^{-1}) to the D band (1330−1360 cm^{-1}), which was represented as I_G/I_D.[54] The density of SWCNTs was low, and the G band was occasionally not observed in the high-temperature synthesis case. Thus, the growth yield of SWCNTs was evaluated through the observation frequency of the G band (the number of appearances of the G band in the measured spectra divided by the total number of measurements). Typically, Raman spectra of 100 spots were collected for the evaluation of the G band observation frequency. Note that more measurement spots were used to determine the G-band observation frequency than that for averaging Raman spectra to ensure the accuracy of the G-band observation frequency even for samples with low-density SWCNTs. Scanning electron microscopy (SEM) (NVision, Carl Zeiss and S-4800, Hitachi) was used for morphology observations of SWCNTs with an acceleration voltage of 1 kV.

3. RESULTS AND DISCUSSION

3.1. Effects of Temperature and C_2H_2 Partial Pressure in the Initial Growth Step. To improve the growth efficiency of cap structures from solid carbon nanoparticles as growth seeds, SWCNT growth was performed under various initial growth conditions while omitting the secondary growth step. To magnify the difference of the growth results, the growth time of the initial growth step was preliminarily set at 2 min. Figure 2 presents the influence of the growth temperature and the partial pressure of carbon feedstock during the initial growth step.

The Raman spectra in Figure 2a show the variations of the SWCNT growth results only with an initial growth step at temperatures of 850 and 900 °C. For the same carbon source partial pressure (1 Pa) and growth time (2 min), the sample synthesized at 900 °C shows a higher intensity of the G band than that synthesized at 850 °C. Since the G band intensity reflects the amount of SWCNTs in the measurement area, its increase indicates that the initial growth efficiency of SWCNTs improves as the temperature increases from 850 to 900 °C. The D band peaks, which originate from structural defects formed on SWCNTs and/or a-C deposited on the surface of SWCNTs and substrates, are observed in both samples. On the other hand, the D band peaks are not observed from the control samples without ND deposition (blank samples, Figure 2a, dotted lines). The absence of the D band from the blank samples suggests that the D band of the SWCNT samples is mostly rooted in defects formed on SWCNTs instead of a-C, which can also be deposited on blank samples. The higher G band and D band intensity from the sample synthesized at 900

https://doi.org/10.1021/acsomega.1c06268
ACS Omega 2022, 7, 3639−3648

°C implies that stationary growth of SWCNTs may begin with a higher growth efficiency even in the initial growth step. The earlier start of stationary growth may be responsible for the quality degradation of SWCNTs obtained at 900 °C, which will be discussed in Section 3.2.

The influences of the growth temperature and the carbon source partial pressure on the growth yield of SWCNTs were examined by recording the G band observation frequencies of the samples grown at 850 and 900 °C and at 0.5 and 1 Pa, as shown in Figure 2b. The increase in the growth temperature from 850 to 900 °C results in an obvious improvement in the growth yield. It should be noted that the yield of SWCNTs grown at 900 °C decreases when the partial pressure of C_2H_2 is slightly increased from 0.5 to 1 Pa. The decrease in the growth efficiency as the carbon supply increases at high temperatures may be related to the deposition of a-C around the growth seeds. Because the growth seed nanoparticles should possess a high surface energy compared with flat SiO_2/Si substrate, a-C is more easily adsorbed on SWCNT growth samples with growth seeds than blank samples. This explains why almost no D band appears on the blank samples but a small amount of a-C is deposited on the SWCNT samples (Figure 2a, dotted line). At the higher temperature for cap formation, the increase of carbon source partial pressure helps to enhance the growth driving force, which makes it easier to overcome the activation barrier for the nucleation of SWCNT caps. Since a higher growth driving force also makes it easier to meet the growth threshold of a-C, a higher temperature accelerates the deposition of a-C. The faster formation rate of a-C on the growth surface lowers the growth efficiency of the cap structure and hinders its lift-off from the nanoparticle. In the case of growth at higher temperatures above 900 °C, the increase of the carbon source partial pressure enhances the deposition rate of a-C on the surface of the growth seeds. Thus, part of the growth seeds is deactivated ahead of time even when the initial growth is not finished, which results in a decrease in the growth yield.

The effect of the carbon source partial pressure in the initial growth step was examined over a wider range from 0.5 to 5 Pa at 850 °C for 2 min. Figure 2c shows the Raman spectra of the samples. The weak G band intensity observed for the samples grown with C_2H_2 partial pressures of 0.5 and 1 Pa indicates that the initial nucleation of SWCNT caps already occurs but few SWCNTs move into the next growth stage in which nanotubes elongate stationarily. When the partial pressure of C_2H_2 is increased to 2.5 or 5 Pa, the G band and D band intensities obviously increase. Cap structures of SWCNTs, which are a hemispherical carbon cage similar to half of a C_{60} molecule, are expected to exhibit no detectable Raman signals in the same wavenumber region as the G and D bands.[55] Therefore, the stronger G and D band intensity indicates that most of SWCNTs have already entered into the stationary elongation stage in the case of 2.5 or 5 Pa. Unlike the growth at 900 °C, the surface of the growth seeds remains clean at a slower a-C deposition rate of 850 °C, which allows for enough time to finish the nucleation procedure (Figure 2a). In the meantime, the increased carbon source partial pressure oversupplies carbon atoms to the growth seeds during the initial growth step, which results in the early start of stationary growth even at the lower growth temperature and the formation of defective SWCNTs (Figure 2c, 2.5 and 5 Pa).

The experimental results for the growth temperature and the carbon source partial pressure suggest that the initial growth step should be well controlled to achieve a high nucleation efficiency of cap structures and, at the same time, further stationary growth of SWCNTs should be avoided during this step. Thus, the initial growth process conducted at 850 °C with 1 Pa C_2H_2 is suitable for further yield improvements of high-quality SWCNTs and is employed in the later experiments. It should be noted that the solid carbon nanoparticles employed as growth seeds in this study do not possess a high catalytic activity, which largely differs from conventional metal catalysts. Hence, the carbon feedstock concentration has to be controlled with high precision to realize efficient SWCNT growth, especially in the cap nucleation stage.

3.2. Two-Step Growth of SWCNTs and Diameter Variations. In the SWCNT growth process, the diameter of SWCNTs is determined mainly by the formed cap structure. Therefore, different nucleation rates of SWCNTs with various diameters were studied indirectly by characterizing the SWCNT tube diameter through radial breathing modes (RBMs) in the Raman spectra (Figure 2d). Samples were synthesized only with the initial growth step at 850 °C for 2 or 10 min. A sample grown with the secondary growth step at 1000 °C for 30 min after initial growth at 850 °C for 2 min was also examined. Comparison of the samples synthesized at 850 °C for 2 and 10 min indicates that the RBM peaks mainly appear at ∼130, ∼180, and ∼270 cm^{-1} in the 10 min case but the RBM peak appears only at ∼130 cm^{-1} in the 2 min case. This difference represents the growth behavior of SWCNTs as a function of diameter. The thicker SWCNTs, which show the RBM peak at 130 cm^{-1}, finish their nucleation and gradually enter into stationary growth in the first 2 min.

The diameter dependence of cap nucleation can be explained well by the regulation of $\Delta\mu$, the difference between $\mu_{C(gas)}$ and $\mu_{C(solid)}$. The variation of $\mu_{C(gas)}$ and $\mu_{C(solid)}$ is related to growth conditions such as temperature and carbon source partial pressure. Besides, the thermodynamic parameters need to be adjusted for different crystal structures of SWCNTs, such as the cap structures and the tube structures with different diameters, which own different strain energy. As reported previously,[24] in an actual reaction, reactants in the gas phase are not in their standard state, and also strain energy should be considered. Thus, at a constant temperature, the growth driving force for carbon feedstock converting into an SWCNT (cap and tube) is expressed as

$$\Delta\mu = \Delta\mu^\circ + \frac{1}{2}k_B T \ln\left(\frac{P_{C_2H_2}}{P_{H_2}}\right) - \frac{A}{d^2} \quad (1)$$

where "°", k_B, d, and A/d^2 represent the standard state, Boltzmann constant, diameter, and strain energy, respectively. The chemical potential $\mu_{C(solid)}$ of SWCNT is influenced by the strain energy, which depends on a part of the SWCNT (cap or tube structures) and the diameter. The constant A differs depending on the cap or the tube structure.

Due to the higher strain energy, the SWCNT cap structure presents higher $\mu_{C(solid)}$ than the tube structure, which is similar to the higher $\mu_{C(solid)}$ for thinner SWCNTs than thicker SWCNTs. Therefore, under the same growth conditions (temperature and partial pressure of C_2H_2), $\Delta\mu$ for stationary elongation of the tube structure is higher than that for cap formation and that for thicker SWCNT formation is higher than that for thinner SWCNT formation (Figure S4). According to the above discussion, for the initial growth step, $\Delta\mu$ provided by the growth condition must meet the

https://doi.org/10.1021/acsomega.1c06268
ACS Omega 2022, 7, 3639−3648

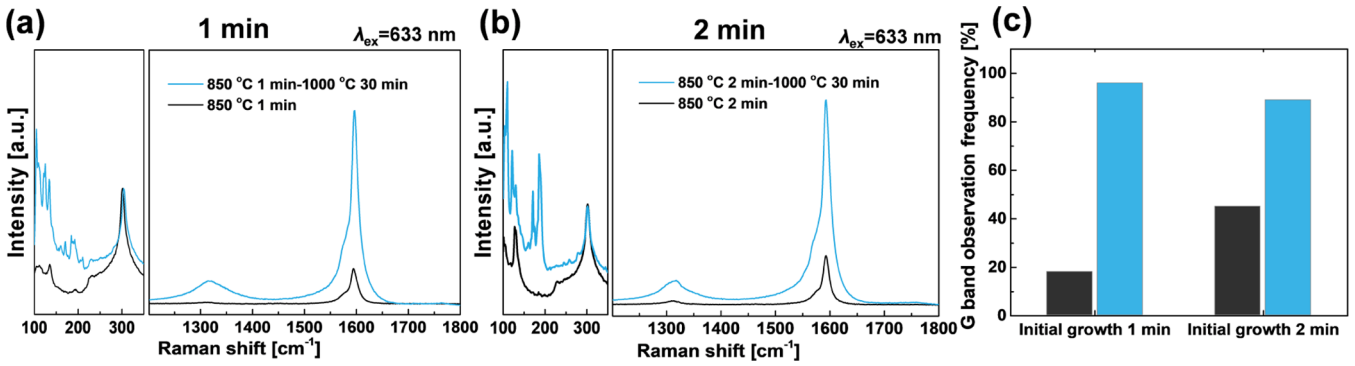

Figure 3. (a, b) Raman spectra of SWCNTs grown with different initial growth times of (a) 1 min and (b) 2 min at 850 °C and 1 Pa, with (blue line) and without (black line) the secondary growth step at 1000 °C and 0.5 Pa for 30 min. (c) G band observation frequency of the four samples with (blue bar) and without (black bar) the secondary growth step.

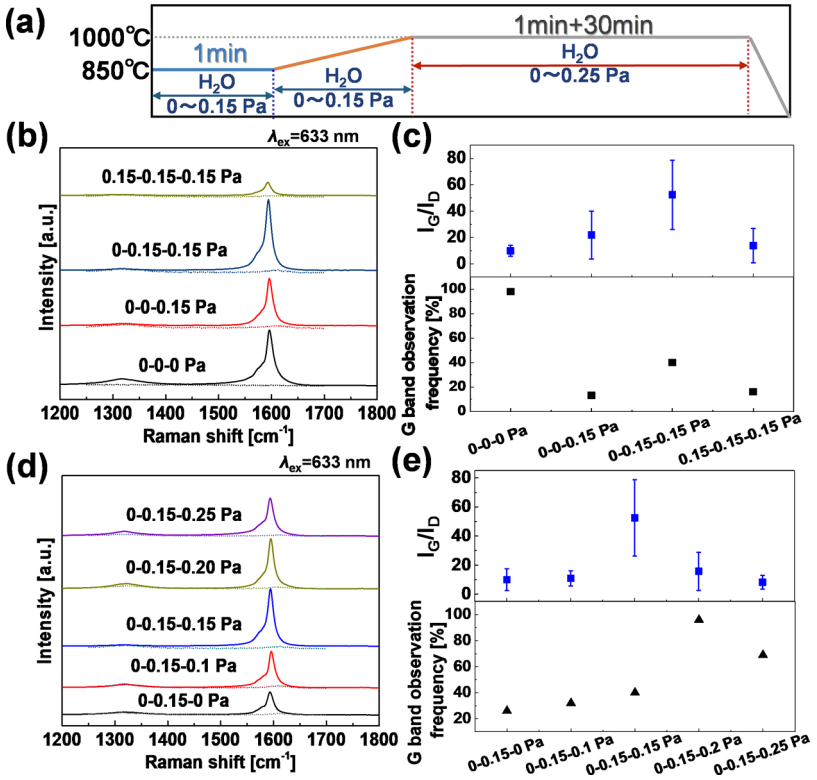

Figure 4. (a) Profiles of temperature and water vapor partial pressure for the SWCNT two-step growth process with water vapor injection. (b) Raman spectra of SWCNTs grown with different timings of water vapor supply: without water vapor throughout the processes (0−0−0 Pa), without water vapor during the temperature rising step and supplying it during the secondary growth step at 0.15 Pa (0−0−0.15 Pa), supplying water vapor both during the temperature rising step and the secondary growth step at 0.15 Pa (0−0.15−0.15 Pa), and supplying water vapor during the whole process at 0.15 Pa (0.15−0.15−0.15 Pa). Growth temperature, partial pressure of C_2H_2, and growth time for the initial growth step are fixed at 850 °C, 1 Pa, and 1 min, respectively, while those for the secondary growth step are 1000 °C, 0.5 Pa, and 30 min, respectively. Dotted lines denote Raman spectra of the blank samples. (c) G band observation frequency and I_G/I_D ratio of the same samples as (b), which reflect the SWCNT yield and quality, respectively. Standard deviation was also calculated and presented as the error bar of averaged I_G/I_D. (d) Raman spectra of SWCNTs grown with different partial pressures of water vapor for both the temperature rising step and the secondary growth step. Dotted lines denote Raman spectra of blank samples. (e) Corresponding G band observation frequency and I_G/I_D, which reflect the SWCNT yield and quality, respectively. Standard deviation was also calculated and presented as the error bar of averaged I_G/I_D.

threshold of the driving force required for nucleation of the cap structures. The initial growth step at 850 °C for 2 min represents a higher growth efficiency for thicker SWCNTs, which have a higher $\Delta\mu$ (Figure 2d, black line). In the case of the only initial growth step, once the nucleation stage is finished, the reduction of $\mu_{C(solid)}$ for the tube increases $\Delta\mu$ for stationary elongation under the same growth condition (Figure 2e). Such an increase makes $\Delta\mu$ fit the threshold for elongation of thinner SWCNTs. On the other hand, this increase can also result in a slight excess of $\Delta\mu$ for elongation of thicker SWCNTs, which is above the growth window (Figure 2f). This leads to the increased possibility of a-C formation, resulting in a decrease in the efficiency of stationary elongation. This growth mechanism explains the result of the stationary elongation stage after the cap formation stage only with the initial growth step for the longer time (10 min), which shows a

https://doi.org/10.1021/acsomega.1c06268
ACS Omega 2022, 7, 3639−3648

delayed formation of thinner SWCNTs with RBM peak at ~270 cm^{-1} and the appearance of stronger RBM peak at ~180 cm^{-1} than that at ~130 cm^{-1} (Figure 2d, red line). If we consider the two-step growth process, after the initial growth, both the increase in the growth temperature and the decrease in the carbon source partial pressure cause the decrease of $\mu_{C(gas)}$ (Figure 2g). Additionally, $\mu_{C(solid)}$ also decreases due to the structural change from a cap to a tube. These decreases make $\Delta\mu$ for stationary elongation during the secondary growth step similar to or lower than that for cap formation during the initial growth step (Figure 2h). Such variation of the growth driving force contributes to the stronger RBM peak at ~130 cm^{-1} and almost no RBM peak at ~270 cm^{-1} (Figure 2d, blue line).

3.3. Effect of Growth Time in the Initial Growth Step. The growth behavior of SWCNTs was also studied by changing the initial growth time. Figure 3a,b shows the Raman spectra of the samples synthesized at 850 °C with the initial growth step of 1 and 2 min with and without the secondary growth step of 30 min, respectively. In the case of only initial growth, a small D band appears from the 2 min sample, whereas the D band from the 1 min sample is negligible. Considering that the blank sample does not show a D band (Figure 2a, black dotted line), a-C deposition does not occur even with 2 min. These results indicate that the D-band from the 2 min sample originates from the defects and that the formation of defects begins after the initial growth of 1 min.

Furthermore, the RBM peaks of the samples synthesized with the secondary growth step at a high temperature exhibit information on the temporal evolution of SWCNTs with different diameters. By conducting the secondary growth step after the initial growth step of 1 or 2 min, a stronger RBM peak around ~180 cm^{-1} emerges, which represents the extra formation of thinner SWCNTs (Figure 3a,b). Since SWCNTs are grown from solid nanoparticles which keep stable morphology at high temperature, diameters of SWCNTs are defined at the stage of cap structure formation and should remain unchanged during the later growth stage. Thus, such extra formation of thinner SWCNTs reflects that the higher amount of smaller size cap structures is formed while prolonging initial growth time. Compared with the 1 min initial growth, the higher RBM peak intensity at ~180 cm^{-1} for the 2 min initial growth indicates a delay in thinner SWCNT growth. The results confirm the diameter dependence of the nucleation timing of SWCNTs in the cap formation stage, which was discussed in Figure 2d previously.

Besides, the growth rate of SWCNTs with different thicknesses can be discussed. As shown in Figure 3a,b, the RBM peak around ~130 cm^{-1} appears in 1 and 2 min initial growth step when there is no thinner SWCNT formed. This growth delay indicates the slower growth rate of thinner SWCNTs than that of thicker SWCNTs from carbon solid nanoparticles.

The growth yield variation upon adjusting initial growth time is displayed in Figure 3c. Compared with the 1 min initial growth, a smaller increase in the G band observation frequency before and after the secondary growth step is observed for the initial growth of 2 min. This is presumably because the initial growth of SWCNTs for 2 min induces some deposition of a-C around ND particles, reducing the growth efficiency in the subsequent growth step.

3.4. Water Vapor Injection during Two-Step Growth. As the growth temperature increases, it becomes more difficult to avoid the formation of a-C on the surface of growth seeds just by adjusting the supply rate of carbon feedstock. To prevent the deposition of a-C, water vapor[15,46] was used to eliminate such deposition via an oxidization reaction. The etching result was analyzed while controlling the injection time and partial pressure of water vapor. As schematically shown in Figure 4a, the etchant injection time was divided into three cases: the addition of water vapor at the beginning of the initial growth step (Figure 4a, process 1), the addition of the etchant at the beginning of the temperature rising step (process 2), and the water vapor addition at the beginning of the secondary growth step (process 3). Additionally, the etchant concentration was separately controlled during the temperature rising step and the secondary growth step. Here, samples are named according to the three values of the water vapor pressure for processes 1, 2, and 3. For example, a sample grown without water vapor during processes 1 and 2 and with the addition of water vapor at 0.15 Pa during process 3 is represented by 0−0−0.15 Pa. As for the other growth parameters, the optimized conditions in the previous section were employed for the initial growth strep (850 °C with 1 Pa C_2H_2 for 1 min) and the secondary growth step (1000 °C with 0.5 Pa C_2H_2 for 30 min).

The decrease in the D band intensity with the injection of etchant demonstrates that water vapor helps prevent the formation of a-C, although the timing of water vapor injection affects the quality (I_G/I_D ratio in Figure 4b) and quantity (G band observation frequency in Figure 4c) of SWCNTs. Compared with the case in which water vapor is injected from the secondary growth step (0−0−0.15 Pa), the case in which the injection time is set at the beginning of the temperature rising step (0−0.15−0.15 Pa) exhibits a higher purity of SWCNTs with a smaller a-C deposition, as indicated by the lower D band intensity. It should be noted that the effect of the water vapor concentration was separately examined for the case of water vapor injection from the secondary growth step (Figure S5). As Figure S5 shows, even when varying the concentration, water vapor cannot etch all of the deposited a-C. a-C may be partly formed before the water vapor injection time during the period where temperature rises to 1000 °C.

Water vapor was also injected from the beginning of the initial growth step (0.15−0.15−0.15 Pa). Compared with water vapor injection from the end of the initial growth step, the case where water vapor participated in the whole growth process exhibits an obvious decrease in the growth yield according to the G band observation frequency and the G band intensity. Such a reduction of the growth yield reflects the negative effect of water vapor on SWCNT nucleation. It has been reported that the cap of SWCNTs is more easily oxidized and consequently destroyed than the sidewall due to the strain and the pentagonal rings of the cap structure.[56] These results indicate that the starting time of etchant injection should begin as soon as possible once the formation of cap structures is finished when etchant is employed in a solid carbon seed-based growth system to prevent a-C deposition and to enhance growth yield.

The I_G/I_D ratio in Figure 4d and the G band observation frequency in Figure 4e show the effect of water vapor etching as a function of partial pressures on the quality and quantity of SWCNTs. While the partial pressure of water vapor during the temperature rising step was fixed at 0.15 Pa, that during the secondary growth step at 1000 °C was varied from 0 to 0.25 Pa. From 0 to 0.15 Pa (0−0.15−0, 0−0.15−0.1, and 0−0.15−

https://doi.org/10.1021/acsomega.1c06268
ACS Omega 2022, 7, 3639−3648

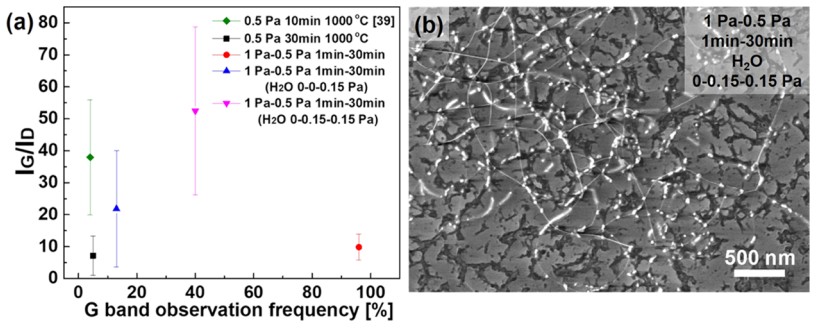

Figure 5. (a) Variations of the growth yield (G band observation frequency) and quality (I_G/I_D ratio) of SWCNTs according to the control of the initial growth conditions and the addition of water vapor in the high-temperature synthesis procedure. Standard deviation was also calculated and presented as the error bar of averaged I_G/I_D. (b) SEM image of SWCNTs grown from two-step growth with water vapor injection, where the initial growth step is conducted at 850 °C and 1 Pa for 1 min followed by the secondary growth step at 1000 °C and 0.5 Pa for 30 min. Water vapor was injected with 0.15 Pa from the beginning in the temperature rising step.

0.15 Pa), both I_G/I_D and the G band observation frequency show a rising tendency with the partial pressure, indicating efficient etching of a-C induced by the participation of water vapor. On the other hand, increasing the partial pressure to 0.2 Pa (0−0.15−0.2 Pa), even though growth yield is further increased, the quality of SWCNTs decreases considerably, and both the quality and the yield decrease when the partial pressure continues to increase to 0.25 Pa (0−0.15−0.25 Pa). Since no obvious D band appears in the Raman spectra of the relevant blank samples, the D band of the SWCNTs grown with water vapor of 0.2 and 0.25 Pa is attributed not to a-C but to the formation of structural defects of SWCNTs. Similar to a previous study using metal nanoparticles,[57] this result suggests that an excess of water vapor damages the SWCNT structures during the growth process but it keeps the surface of growth seeds free from a-C and enhances the SWCNT yield. In addition, as mentioned earlier, a further increase of SWCNT yield appeared in the case of excessive water injection concentration (0−0.15−0.2 Pa), in which the quality of SWCNTs decreased. This phenomenon in the VSSS growth mode brings the possibility to discuss the etching site by water vapor, that is, a-C on carbon growth seeds or the edges of SWCNTs. If we assume the edge of newly grown SWCNTs is preferentially etched by water, the growth rate would be sensitive to etchant concentration and more likely to decrease once the partial pressure of water vapor is increased to more than 0.15 Pa. However, the experiment provided an opposite result, an increased yield of SWCNTs. Thus, we speculate that water vapor tends to etch a-C randomly on the growth seed surface. Further study is needed to elucidate the atomistic mechanism of water in the VSSS mode in the future.

The interpretation of the growth results with the water vapor addition provides a practical direction for the efficient growth of SWCNTs from solid growth seeds. Through the reaction between water vapor and a-C, excessive deposition of carbon source on the growth seed surface is controlled, which therefore enhanced the lifetime of growth seeds. The addition of water vapor just after the formation of cap structures and the precise adjustment of the concentration of etchant are keys to obtain high-quality SWCNTs with a high yield.

3.5. Yield and Quality of SWCNTs Synthesized under Different Growth Conditions. Figure 5a compares the yield and the quality of SWCNTs grown under various conditions from solid carbon particles as growth seeds. Compared with previous research on one-step growth at 1000 °C,[39] cap engineering using the two-step growth process developed in this study significantly improves the growth yield, although the deposition of a-C, which reduces I_G/I_D, remains. To solve this impurity problem, water vapor was employed as an etchant to keep the surface of growth seeds clean. We successfully obtained highly crystalline SWCNTs with a higher growth yield, which have I_G/I_D of ∼52 and a G band observation frequency of 40%. The value of the G band observation frequency demonstrates a significant improvement from the previous work of 4%.[39] This result demonstrates the effectiveness of the two-step growth process combined with water vapor addition.

Figure 5b shows the SEM image of SWCNTs grown by the two-step growth process with water vapor injection. Supported by carbon nanoparticle seeds (light gray particles in Figure 5b), SWCNTs with a length of a few micrometers are observed. The SWCNT density of the samples well corresponds to the values of the G band observation frequency. It should be noted that the length of SWCNTs is limited by the relatively low efficiency of SWCNT growth at a high temperature. Based on the present achievement to enhance the cap formation, future studies on prolonging the growth lifetime of SWCNTs from solid carbon nanoparticles should further improve the length and the yield of high-crystallinity SWCNTs.

4. CONCLUSIONS

In conclusion, we developed a cap formation-engineered two-step growth process of SWCNTs from solid carbon nanoparticles at a high temperature by considering the growth driving forces in different growth stages. We successfully grew highly crystalline SWCNTs with improved yields. In this growth system, we mainly concentrated on the initial growth efficiency, which significantly influences the quality and quantity of the resulting SWCNTs. To fit the higher growth driving force needed for cap structure formation, a higher partial pressure of carbon source was selected for the initial growth step. The effects of growth temperature and time for the initial growth step were also systematically examined to prevent the deposition of a-C and to control the formation of SWCNT caps. After achieving a higher nucleation density of the cap structures, stationary elongation of SWCNTs was conducted by a secondary growth step. Furthermore, the deposition of a-C at high temperatures was eliminated by supplying an etchant, water vapor, to the growth system. By investigating the injection time and the concentration of water vapor, we optimized the condition for efficiently removing a-C

https://doi.org/10.1021/acsomega.1c06268
ACS Omega 2022, 7, 3639−3648

while preserving the nucleation of the cap structures. We significantly improved the growth yield, as evidenced by the increase of the G band observation frequency from 4 to 40% while maintaining a high I_G/I_D ratio of 52. Our results provide a rational guideline to synthesize high-quality SWCNTs using high-temperature-stable solid carbon nanoparticles as growth seeds and will enable various high-end applications based on SWCNTs that are free from metal impurities, defects, and a-C.

■ ASSOCIATED CONTENT

Supporting Information

The Supporting Information is available free of charge at https://pubs.acs.org/doi/10.1021/acsomega.1c06268.

Investigation of possible SWCNT growth from impurity in ND (Figure S1); characterization of ND size before and after heating in air (600 °C 10 min) (Figure S2); schematic model and reaction coordinate of the CVD growth process of SWCNTs from solid carbon nanoparticles under different conditions (Figure S3); relationship between SWCNT growth driving force and growth stages as well as SWCNT diameters (Figure S4); and investigation of SWCNT growth results with adding different partial pressures of water vapor at the beginning of the secondary growth step (Figure S5) (PDF)

■ AUTHOR INFORMATION

Corresponding Author

Yoshihiro Kobayashi − *Department of Applied Physics, Osaka University, Suita, Osaka 565-0871, Japan*; Phone: +81 06 6879 7833; Email: kobayashi@ap.eng.osaka-u.ac.jp; Fax: +81 06 6879 7863

Authors

Mengyue Wang − *Department of Applied Physics, Osaka University, Suita, Osaka 565-0871, Japan*; orcid.org/0000-0001-9106-6125

Keisuke Nakamura − *Department of Applied Physics, Osaka University, Suita, Osaka 565-0871, Japan*

Michiharu Arifuku − *Nippon Kayaku Co., Ltd., Tokyo 115-8588, Japan*

Noriko Kiyoyanagi − *Nippon Kayaku Co., Ltd., Tokyo 115-8588, Japan*

Taiki Inoue − *Department of Applied Physics, Osaka University, Suita, Osaka 565-0871, Japan*; orcid.org/0000-0003-1739-917X

Complete contact information is available at: https://pubs.acs.org/10.1021/acsomega.1c06268

Notes

The authors declare no competing financial interest.

■ ACKNOWLEDGMENTS

The authors would like to thank Dr. T. Sakata of Research Center for Ultra-High Voltage Electron Microscopy, Osaka University, for assistance with the SEM observation. The part of this work was financially supported by JSPS KAKENHI (grant numbers JP15H05867 and JP17H02745) and JST SPRING. This work was also supported by Nanotechnology Platform Project of MEXT (grant number JPMXP09F21OS0023).

■ REFERENCES

(1) Iijima, S. Helical microtubules of graphitic carbon. *Nature* **1991**, *354*, 56−58.

(2) Yu, M.-F.; Lourie, O.; Dyer, M. J.; Moloni, K.; Kelly, T. F.; Ruoff, R. S. Strength and Breaking Mechanism of Multiwalled Carbon Nanotubes Under Tensile Load. *Science* **2000**, *287*, 637.

(3) Tans, S. J.; Verschueren, A. R. M.; Dekker, C. Room-temperature transistor based on a single carbon nanotube. *Nature* **1998**, *393*, 49−52.

(4) Pop, E.; Mann, D.; Wang, Q.; Goodson, K.; Dai, H. Thermal Conductance of an Individual Single-Wall Carbon Nanotube above Room Temperature. *Nano Lett.* **2006**, *6*, 96−100.

(5) Iijima, S.; Ichihashi, T. Single-shell carbon nanotubes of 1-nm diameter. *Nature* **1993**, *363*, 603−605.

(6) Hills, G.; Lau, C.; Wright, A.; Fuller, S.; Bishop, M. D.; Srimani, T.; Kanhaiya, P.; Ho, R.; Amer, A.; Stein, Y.; et al. Modern microprocessor built from complementary carbon nanotube transistors. *Nature* **2019**, *572*, 595−602.

(7) Kong, J.; Franklin, N. R.; Zhou, C.; Chapline, M. G.; Peng, S.; Cho, K.; Dai, H. Nanotube Molecular Wires as Chemical Sensors. *Science* **2000**, *287*, 622.

(8) He, X.; Htoon, H.; Doorn, S. K.; Pernice, W. H. P.; Pyatkov, F.; Krupke, R.; Jeantet, A.; Chassagneux, Y.; Voisin, C. Carbon nanotubes as emerging quantum-light sources. *Nat. Mater.* **2018**, *17*, 663−670.

(9) Saito, R.; Fujita, M.; Dresselhaus, G.; Dresselhaus, M. S. Electronic structure of chiral graphene tubules. *Appl. Phys. Lett.* **1992**, *60*, 2204−2206.

(10) Arora, N.; Sharma, N. N. Arc discharge synthesis of carbon nanotubes: Comprehensive review. *Diamond Relat. Mater.* **2014**, *50*, 135−150.

(11) Thess, A.; Lee, R.; Nikolaev, P.; Dai, H.; Petit, P.; Robert, J.; Xu, C.; Lee, Y. H.; Kim, S. G.; Rinzler, A. G.; et al. Crystalline Ropes of Metallic Carbon Nanotubes. *Science* **1996**, *273*, 483.

(12) Dai, H.; Rinzler, A. G.; Nikolaev, P.; Thess, A.; Colbert, D. T.; Smalley, R. E. Single-wall nanotubes produced by metal-catalyzed disproportionation of carbon monoxide. *Chem. Phys. Lett.* **1996**, *260*, 471−475.

(13) Yoshida, H.; Takeda, S.; Uchiyama, T.; Kohno, H.; Homma, Y. Atomic-Scale In-situ Observation of Carbon Nanotube Growth from Solid State Iron Carbide Nanoparticles. *Nano Lett.* **2008**, *8*, 2082−2086.

(14) Nikolaev, P.; Bronikowski, M. J.; Bradley, R. K.; Rohmund, F.; Colbert, D. T.; Smith, K. A.; Smalley, R. E. Gas-phase catalytic growth of single-walled carbon nanotubes from carbon monoxide. *Chem. Phys. Lett.* **1999**, *313*, 91−97.

(15) Hata, K.; Futaba, D. N.; Mizuno, K.; Namai, T.; Yumura, M.; Iijima, S. Water-Assisted Highly Efficient Synthesis of Impurity-Free Single-Walled Carbon Nanotubes. *Science* **2004**, *306*, 1362−1364.

(16) Yang, F.; Wang, X.; Zhang, D.; Yang, J.; Luo, D.; Xu, Z.; Wei, J.; Wang, J.-Q.; Xu, Z.; Peng, F.; et al. Chirality-specific growth of single-walled carbon nanotubes on solid alloy catalysts. *Nature* **2014**, *510*, 522−524.

(17) He, M.; Wang, X.; Zhang, S.; Jiang, H.; Cavalca, F.; Cui, H.; Wagner, J. B.; Hansen, T. W.; Kauppinen, E.; Zhang, J.; et al. Growth kinetics of single-walled carbon nanotubes with a (2*n*,*n*) chirality selection. *Sci. Adv.* **2019**, *5*, No. eaav9668.

(18) Charlier, J. C.; Ebbesen, T. W.; Lambin, P. Structural and electronic properties of pentagon-heptagon pair defects in carbon nanotubes. *Phys. Rev. B* **1996**, *53*, 11108−11113.

(19) Senga, R.; Pichler, T.; Yomogida, Y.; Tanaka, T.; Kataura, H.; Suenaga, K. Direct Proof of a Defect-Modulated Gap Transition in Semiconducting Nanotubes. *Nano Lett.* **2018**, *18*, 3920−3925.

(20) Choi, H. J.; Ihm, J.; Louie, S. G.; Cohen, M. L. Defects, quasibound states, and quantum conductance in metallic carbon nanotubes. *Phys. Rev. Lett.* **2000**, *84*, 2917.

(21) Suzuki, S.; Kobayashi, Y. Conductivity decrease in carbon nanotubes caused by low-acceleration-voltage electron irradiation. *Jpn. J. Appl. Phys.* **2005**, *44*, L1498.

(22) Yamamoto, T.; Watanabe, K. Nonequilibrium Green's Function Approach to Phonon Transport in Defective Carbon Nanotubes. *Phys. Rev. Lett.* **2006**, *96*, No. 255503.
(23) Sammalkorpi, M.; Krasheninnikov, A.; Kuronen, A.; Nordlund, K.; Kaski, K. Mechanical properties of carbon nanotubes with vacancies and related defects. *Phys. Rev. B* **2004**, *70*, No. 245416.
(24) Vinten, P.; Marshall, P.; Lefebvre, J.; Finnie, P. Thermodynamic and Energetic Effects on the Diameter and Defect Density in Single-Walled Carbon Nanotube Synthesis. *J. Phys. Chem. C* **2013**, *117*, 3527−3536.
(25) Yuan, Q.; Xu, Z.; Yakobson, B. I.; Ding, F. Efficient Defect Healing in Catalytic Carbon Nanotube Growth. *Phys. Rev. Lett.* **2012**, *108*, No. 245505.
(26) Tibbetts, G. G. Vapor-grown carbon fibers: Status and prospects. *Carbon* **1989**, *27*, 745−747.
(27) Harutyunyan, A. R.; Pradhan, B. K.; Kim, U. J.; Chen, G.; Eklund, P. C. CVD Synthesis of Single Wall Carbon Nanotubes under "Soft" Conditions. *Nano Lett.* **2002**, *2*, 525−530.
(28) Altay, M. C.; Eroglu, S. Synthesis of multi-walled C nanotubes by Fe−Ni (70wt.%) catalyzed chemical vapor deposition from pre-heated CH4. *Mater. Lett.* **2012**, *67*, 124−127.
(29) Bethune, D. S.; Kiang, C. H.; de Vries, M. S.; Gorman, G.; Savoy, R.; Vazquez, J.; Beyers, R. Cobalt-catalysed growth of carbon nanotubes with single-atomic-layer walls. *Nature* **1993**, *363*, 605−607.
(30) Chiang, W.-H.; Mohan Sankaran, R. Linking catalyst composition to chirality distributions of as-grown single-walled carbon nanotubes by tuning NixFe1−x nanoparticles. *Nat. Mater.* **2009**, *8*, 882−886.
(31) Kim, S. M.; Pint, C. L.; Amama, P. B.; Zakharov, D. N.; Hauge, R. H.; Maruyama, B.; Stach, E. A. Evolution in Catalyst Morphology Leads to Carbon Nanotube Growth Termination. *J. Phys. Chem. Lett.* **2010**, *1*, 918−922.
(32) Hersam, M. C. Progress towards monodisperse single-walled carbon nanotubes. *Nat. Nanotechnol.* **2008**, *3*, 387−394.
(33) Takagi, D.; Hibino, H.; Suzuki, S.; Kobayashi, Y.; Homma, Y. Carbon Nanotube Growth from Semiconductor Nanoparticles. *Nano Lett.* **2007**, *7*, 2272−2275.
(34) Zhang, S.; Kang, L.; Wang, X.; Tong, L.; Yang, L.; Wang, Z.; Qi, K.; Deng, S.; Li, Q.; Bai, X.; et al. Arrays of horizontal carbon nanotubes of controlled chirality grown using designed catalysts. *Nature* **2017**, *543*, 234−238.
(35) Liu, H.; Takagi, D.; Ohno, H.; Chiashi, S.; Chokan, T.; Homma, Y. Growth of Single-Walled Carbon Nanotubes from Ceramic Particles by Alcohol Chemical Vapor Deposition. *Appl. Phys. Express* **2008**, *1*, No. 014001.
(36) Qian, L.; Xie, Y.; Yu, Y.; Wang, S.; Zhang, S.; Zhang, J. Growth of Single-Walled Carbon Nanotubes with Controlled Structure: Floating Carbide Solid Catalysts. *Angew. Chem., Int. Ed.* **2020**, *59*, 10884−10887.
(37) Homma, Y.; Liu, H.; Takagi, D.; Kobayashi, Y. Single-walled carbon nanotube growth with non-iron-group "catalysts" by chemical vapor deposition. *Nano Res.* **2009**, *2*, No. 793.
(38) Takagi, D.; Kobayashi, Y.; Homma, Y. Carbon Nanotube Growth from Diamond. *J. Am. Chem. Soc.* **2009**, *131*, 6922−6923.
(39) Nakamura, K.et al.Synthesis of Defect-Free Single-Walled Carbon Nanotube from Solid Nanoparticles by High Temperature Process, in preparation, 2022.
(40) Wagg, L. M.; Hornyak, G. L.; Grigorian, L.; Dillon, A. C.; Jones, K. M.; Blackburn, J.; Parilla, P. A.; Heben, M. J. Experimental Gibbs Free Energy Considerations in the Nucleation and Growth of Single-Walled Carbon Nanotubes. *J. Phys. Chem. B* **2005**, *109*, 10435−10440.
(41) Qi, H.; Yuan, D.; Liu, J. Two-Stage Growth of Single-Walled Carbon Nanotubes. *J. Phys. Chem. C* **2007**, *111*, 6158−6160.
(42) Homma, Y.; Kobayashi, Y.; Ogino, T.; Takagi, D.; Ito, R.; Jung, Y. J.; Ajayan, P. M. Role of Transition Metal Catalysts in Single-Walled Carbon Nanotube Growth in Chemical Vapor Deposition. *J. Phys. Chem. B* **2003**, *107*, 12161−12164.
(43) Wagner, R. S.; Ellis, W. C. Vapor-Liquid-Solid Mechanism of Single Crystal Growth. *Appl. Phys. Lett.* **1964**, *4*, 89−90.
(44) Kase, H.; Negishi, R.; Arifuku, M.; Kiyoyanagi, N.; Kobayashi, Y. Biosensor response from target molecules with inhomogeneous charge localization. *J. Appl. Phys.* **2018**, *124*, No. 064502.
(45) Wen, Q.; Zhang, R.; Qian, W.; Wang, Y.; Tan, P.; Nie, J.; Wei, F. Growing 20 cm Long DWNTs/TWNTs at a Rapid Growth Rate of 80−90 μm/s. *Chem. Mater.* **2010**, *22*, 1294−1296.
(46) Yamada, T.; Maigne, A.; Yudasaka, M.; Mizuno, K.; Futaba, D. N.; Yumura, M.; Iijima, S.; Hata, K. Revealing the Secret of Water-Assisted Carbon Nanotube Synthesis by Microscopic Observation of the Interaction of Water on the Catalysts. *Nano Lett.* **2008**, *8*, 4288−4292.
(47) Smajda, R.; Andresen, J. C.; Duchamp, M.; Meunier, R.; Casimirius, S.; Hernádi, K.; Forró, L.; Magrez, A. Synthesis and mechanical properties of carbon nanotubes produced by the water assisted CVD process. *Phys. Status Solidi B* **2009**, *246*, 2457−2460.
(48) Wyss, R. M.; Klare, J. E.; Park, H. G.; Noy, A.; Bakajin, O.; Lulevich, V. Water-Assisted Growth of Uniform 100 mm Diameter SWCNT Arrays. *ACS Appl. Mater. Interfaces* **2014**, *6*, 21019−21025.
(49) Hasegawa, K.; Noda, S. Millimeter-Tall Single-Walled Carbon Nanotubes Rapidly Grown with and without Water. *ACS Nano* **2011**, *5*, 975−984.
(50) Shenderova, O. A.; Gruen, D. M. *Ultrananocrystalline Diamond: Synthesis, Properties and Applications*; William Andrew, 2012.
(51) Gruen, D. M.; Shenderova, O. A.; Vul, A. Y. In *Synthesis, Properties and Applications of Ultrananocrystalline Diamond*, Proceedings of the NATO ARW on Synthesis, Properties and Applications of Ultrananocrystalline Diamond, St. Petersburg, Russia, from 7 to 10 June 2004; Springer Science & Business Media, 2006.
(52) Kuznetsov, V. L.; Chuvilin, A. L.; Butenko, Y. V.; Mal'kov, I. Y.; Titov, V. M. Onion-like carbon from ultra-disperse diamond. *Chem. Phys. Lett.* **1994**, *222*, 343−348.
(53) Kovalenko, I.; Bucknall, D. G.; Yushin, G. Detonation Nanodiamond and Onion-Like-Carbon-Embedded Polyaniline for Supercapacitors. *Adv. Funct. Mater.* **2010**, *20*, 3979−3986.
(54) Belin, T.; Epron, F. Characterization methods of carbon nanotubes: a review. *Mater. Sci. Eng., B* **2005**, *119*, 105−118.
(55) Milani, A.; Tommasini, M.; Russo, V.; Bassi, A. L.; Lucotti, A.; Cataldo, F.; Casari, C. S. Raman spectroscopy as a tool to investigate the structure and electronic properties of carbon-atom wires. *Beilstein J. Nanotechnol.* **2015**, *6*, 480−491.
(56) Ajayan, P. M.; Ebbesen, T. W.; Ichihashi, T.; Iijima, S.; Tanigaki, K.; Hiura, H. Opening carbon nanotubes with oxygen and implications for filling. *Nature* **1993**, *362*, 522−525.
(57) Kimura, H.; Futaba, D. N.; Yumura, M.; Hata, K. Mutual Exclusivity in the Synthesis of High Crystallinity and High Yield Single-Walled Carbon Nanotubes. *J. Am. Chem. Soc.* **2012**, *134*, 9219−9224.

https://doi.org/10.1021/acsomega.1c06268
ACS Omega 2022, 7, 3639−3648